TURBOFAN JET NOISE REDUCTION VIA DEFLECTION OF THE BYPASS STREAM

Dimitri Papamoschou [*]
Kimberley A. Nishi [†]
University of California, Irvine, California 92697-3975

We describe a parametric experimental study of noise reduction via deflection of the secondary stream in dual-stream jets. The jets simulated the exhaust of turbofan engines with bypass ratios 4.5 and 6.0. The secondary (bypass) stream was deflected downward by means of vanes installed inside the bypass duct. Variables included the number of vanes, vane angle of attack, azimuthal placement, and axial position. The shape of the bypass duct was also varied. Noise measurements were converted to estimates of flyover and sideline effective perceived noise level (EPNL). The quietest configurations used a rapidly convergent bypass duct with vanes installed in the proximity of the duct exit. Two pairs of vanes, installed at azimuth angles 70 and 110 deg with respect to the vertical, constitutes one of the most promising configurations. Substantial benefit in EPNL occurs when the vanes have dissimilar angles of attack, with the upper pair at smaller incidence than the lower pair. The best arrangement offered a 5.3-dB reduction in the sum of flyover and sideline EPNL.

Nomenclature

a	=	mean speed of sound
a_{2D}	=	two-dimensional lift curve slope
A	=	duct cross sectional area
B	=	bypass ratio, $\dot{m}_s/\dot{m}_p$
c	=	chord length of vane
C_D	=	total drag coefficient of vane
C_{D_p}	=	parasite drag coefficient of vane
C_L	=	lift coefficient of vanes
D	=	nozzle diameter or total drag of vanes
D_i	=	inviscid induced drag of vanes
f	=	frequency
K	=	induced viscous drag factor
L	=	lift of vanes
$\dot{m}$	=	mass flow rate
M	=	Mach number
M_c	=	convective Mach number
N_v	=	number of vanes
r	=	distance from jet exit
S_v	=	vane planform area
$\mathcal{T}$	=	thrust
u	=	mean velocity in jet plume
U	=	nozzle-exit or internal velocity
U_c	=	convective velocity
w	=	width of vane
α	=	angle of attack (vane or aircraft)
β	=	vane impact coefficient, Eq. 7
γ	=	climb angle
ϵ	=	deflection angle of bypass stream
θ	=	polar angle relative to jet axis
ϕ	=	azimuth angle
ρ	=	density

Subscripts

eng	=	engine
exp	=	experiment
fo	=	flyover
p	=	primary (core) exhaust
s	=	secondary (bypass) exhaust
sl	=	sideline
v	=	vanes
∞	=	flight conditions

[*]Professor, Associate Fellow AIAA
[†]Graduate student, Member AIAA

American Institute of Aeronautics and Astronautics

Introduction

Aircraft noise is an issue of enormous environmental, financial, and technological impact. There are two main sources of noise in today's commercial aircraft engines: fan/compressor noise and jet noise. Jet noise comprises turbulent mixing noise and, in the case of imperfectly expanded jets, shock noise [1]. Turbulent mixing noise is very difficult to control so its suppression remains a challenge. It is generally agreed that turbulent shear-flow mixing causes two types of noise: sound produced by the large-scale eddies and sound generated by the fine-scale turbulence [2]. The former is very intense and directional, and propagates at an angle close to the jet axis. The latter is mostly uniform and affects the lateral and upstream directions.

The increase in bypass ratio over the last three decades has resulted in a dramatic suppression in the jet noise of turbofan engines. Modern engines are so quiet that further reduction in noise becomes extremely challenging. The success of the high-bypass engine is offset, to some degree, by the increasing volume of aircraft operations. This creates more environmental and political pressures for quieter aircraft. Today the most successful technique for reducing jet noise from high-bypass engines involves the installation of chevron mixers on the exhaust nozzles [3]. However, the ever increasing need for quieter engines requires exploration of alternative techniques that could be used by themselves or in conjunction with existing methods. The technique described in this paper targets noise from large-scale eddies.

Large-scale mixing noise has been successfully modeled by treating large eddies as instability waves. The notion of sound radiation from large-scale flow instabilities was first confirmed in the supersonic jet experiments of McLaughlin et al. [4] and the subsequent experiments of Troutt & McLaughlin [5]. In those experiments, the orientation, wavelength, and frequency of the measured acoustic radiation were found to be consistent with the Mach wave concept. The linear stability analysis of Tam & Burton [6] further solidified this idea by showing that the sound emitted by a supersonic wave matched the trends found in the aforementioned experiments. Since then, a large volume of experimental and theoretical works have addressed various aspects of this problem. See for example Refs.[7], [8], and [9].

Mach wave emission is governed by the the convec-

tive Mach number M_c of the instability wave. When M_c is supersonic, strong Mach wave radiation is noticeable in instantaneous photographs of jets. For subsonic M_c, the growth-decay nature of instability waves creates a spectrum of phase speeds, part of which is supersonic [2, 10, 11, 12]. The resulting Mach wave emission is not as intense or nonlinear as its supersonic counterpart but still constitutes the strongest source of sound. As M_c becomes more subsonic, Mach wave emission weakens rapidly. Reduction of M_c thus has the potential of being an effective method for noise suppression. Recent works have demonstrated noise suppression from supersonic jets by application of a parallel secondary flow around the primary jet. The secondary flow reduces the convective Mach number of the primary eddies, hence curtails their ability to generate sound that radiates to the far field. Eccentric nozzle configurations were very effective in this respect because the thick part of the secondary flow covered most of the noise sources on the underside of the jet, hence suppressed downward-emitted sound [13, 14].

It became apparent, however, that offsetting the nozzles to an eccentric geometry did not offer an attractive engineering solution for high-bypass engines. Notwithstanding the possible losses caused by the new flow path, an eccentric arrangement would require a new nacelle structure and radical redesign of propulsion systems such as thrust reversers. An alternative was sought that would provide equal or greater acoustic benefit while minimizing modifications. The most promising configuration involves the use of deflector vanes, installed near the exit of the bypass duct. that cause the bypass plume to tilt relative to the core plume. In effect, this method creates "eccentricity" not at the nozzle exit but further downstream. Application of this method to supersonic- and subsonic-type engines has been described in recent publications [15, 16]. The vane configurations of those studies were ad-hoc, not the result of any optimization. This study involves a parametric variation of the vane and nozzle geometry to generate some insight as to which arrangements are most promising. We also examine the vane aerodynamics in more detail and attempt to extract fundamental trends from the data collected.

American Institute of Aeronautics and Astronautics

Deflection of the Bypass Stream

The rationale for tilting the bypass plume relative to the core plume is to thicken the bypass stream in the vicinity of the strongest sources of noise (largest eddies) of the core stream. Recent noise source location experiments have shown that the strongest sources of noise reside near the end of the primary potential core [17, 18, 19]. Given that the length of the primary potential core is on the order of 15 primary exit diameters, one can make an order-of-magnitude estimate that the desired tilt angle is a modest 1/15 or 4°. The tilt entails a transverse (lift) force L applied to the bypass stream near its exit. Figure 1 shows the basic arrangement. Here we consider generation of this force by vanes immersed in the bypass stream.

The vanes could be placed inside or outside the bypass duct. Placement inside the duct has the advantage of a subsonic environment and thus avoidance of serious shock losses. There is a limit as to how deep inside the duct one should place the vanes: the aerodynamic force of the vanes should be transmitted to the momentum flux exiting the duct and not to the duct walls. Otherwise the effect of vane lift will be lessened or cancelled by transverse forces acting on the duct walls. Assuming that the lift of the vanes is transmitted entirely to the exhaust plume, and that all the flow angles are small, the integral momentum equation gives the following relation between the tilt angle of the bypass stream and the lift force of the vanes:

$$\epsilon = \frac{L}{\dot{m}_s U_s} \qquad (1)$$

The ideal thrust loss of the bypass stream is connected to the cosine of the tilt angle. We can draw an analogy between the ideal thrust loss of the jet and the inviscid induced (lift-dependent) drag of a finite wing. In both instances the momentum flux is deflected downward to generate lift; the tilting of the momentum vector results in induced drag (for a treatment of the finite wing as a flow deflector the reader is referred to [20]). The ideal thrust loss of the jet is thus equal to the inviscid induced drag of the vanes, D_i, given by

$$D_i = \dot{m}_s U_s (1 - \cos \epsilon) \approx \dot{m}_s U_s \frac{\epsilon^2}{2}$$

where the small angle approximation $\cos \epsilon \approx 1 - \frac{1}{2}\epsilon^2$ was used. Combining with Eq. 1,

$$D_i = L \frac{\epsilon}{2} \qquad (2)$$

In the analysis that follows we consider the aerodynamics of vanes installed inside the bypass duct. Figure 2 shows the generic geometry. There are no published works on this type of flow, so the intent of the analysis is to generate some fundamental insight into the basic aerodynamics. We will attempt some predictions of lift and drag with the understanding that these will be preliminary estimates to be confirmed by future computations and experiments. Each vane is assumed to be an airfoil of constant chord c and width w equal to the width of the bypass duct. The planform area of each vanes is $S_v = cw$. The vanes would be typically installed in $N_v/2$ pairs. For each pair, the vanes are installed at azimuth angles $\pm\phi_j$ and angle of attack α_j. The vanes may also have a "dihedral" angle $\delta\phi_j$ as shown on Fig. 2. In the analysis that follows the symbol ϕ_j represents the sum of the azimuthal placement angle plus the dihedral. All the vanes are assumed to have the same planform area and airfoil shape. The lift of a given vane pair is

$$L_j = \frac{1}{2}\rho_v U_v^2 2 S_v C_{L_j} \sin \phi_j \qquad (3)$$

where C_{L_j} is the lift coefficient. The total lift is

$$L = \rho_v U_v^2 S_v \sum_{j=1}^{N_v/2} C_{L_j} \sin \phi_j \qquad (4)$$

Letting

$$\overline{(\cdot)} = \frac{2}{N_v} \sum_{j=1}^{N_v/2} (\cdot)$$

denote the average over all the pairs,

$$L = \frac{1}{2} N_v \rho_v U_v^2 S_v \overline{C_L \sin \phi} \qquad (5)$$

Applying Eq. 1, the deflection of the bypass stream is

$$\epsilon = \frac{N_v S_v U_v}{2 A_v U_s} \overline{C_L \sin \phi} \qquad (6)$$

where the conservation of mass $\dot{m}_s = \rho_s U_s A_s = \rho_v U_v A_v$ was used. Defining the vane impact coefficient as

$$\beta = \frac{1}{4} \frac{N_v S_v}{A_v} \frac{U_v}{U_s} \qquad (7)$$

we have

$$\frac{\epsilon}{2} = \beta \overline{C_L \sin \phi} \qquad (8)$$

Since the airfoil is bounded by sidewalls it would appear that, save for viscous end-wall effects, it behaves as an infinite two-dimensional airfoil. If this

3

were true, and excluding wave drag, there would be no inviscid induced drag. We know, however, that there is a thrust loss, given by Eq. 2, even in the limit of inviscid, shock-free flow. The integral view of the jet, captured by Eqs. 1 and 2, and the detailed view of the vane airfoils can be reconciled by considering $\epsilon/2$ in Eq. 2 as the "downwash" angle in the vicinity of the vanes. To be precise, we should consider the component of downwash velocity normal to the plane of the vane. That is, the effective downwash angle for each vane pair is $(\epsilon \sin \phi_j)/2$. The total drag of each vane pair consists of the parasite drag, the viscous induced drag, and the inviscid induced drag caused by the downwash angle $(\epsilon \sin \phi_j)/2$. Denoting the parasite drag coefficient C_{D_p} (same for all vanes), the viscous induced drag is assumed to scale as $K C_{D_p} C_L^2$ [20]. Thus the drag coefficient of each vane pair is

$$C_{D_j} = C_{D_p} + C_{D_p} K C_{L_j}^2 + C_{L_j} \frac{\epsilon}{2} \sin \phi_j \quad (9)$$

Applying Eq. 8,

$$C_{D_j} = C_{D_p} + C_{D_p} K C_{L_j}^2 + \beta \overline{C_L \sin \phi} C_{L_j} \sin \phi_j \quad (10)$$

The average drag coefficient is

$$\overline{C_D} = C_{D_p} + K C_{D_p} \overline{C_L^2} + \beta (\overline{C_L \sin \phi})^2 \quad (11)$$

and the total drag is

$$D = \frac{1}{2} N_v \rho_v U_v^2 S_v \overline{C_D} \quad (12)$$

Dividing by the total lift given by Eq. 4, the drag-to-lift ratio is

$$\frac{D}{L} = \frac{C_{D_p} + K C_{D_p} \overline{C_L^2} + \beta (\overline{C_L \sin \phi})^2}{\overline{C_L \sin \phi}}$$

Using Eq. 8,

$$\frac{D}{L} = \frac{2 C_{D_p} \beta}{\epsilon} + K C_{D_p} \frac{\overline{C_L^2}}{\overline{C_L \sin \phi}} + \frac{\epsilon}{2} \quad (13)$$

Multiplying by the lift force given by Eq. 1 and using again Eq. 8,

$$D = \dot{m}_s U_s \left[2 C_{D_p} \beta (1 + K \overline{C_L^2}) + \frac{\epsilon^2}{2} \right] \quad (14)$$

To obtain the total drag of the vanes as a fraction of the total thrust, Eq. 18 is divided by $\mathcal{T}_{\text{total}} = \dot{m}_p(U_p - U_\infty) + \dot{m}_s(U_s - U_\infty)$ to give

$$\frac{D}{\mathcal{T}_{\text{total}}} = \left[2 C_{D_p} \beta (1 + K \overline{C_L^2}) + \frac{\epsilon^2}{2} \right] \times$$
$$\frac{B U_s}{U_p - U_\infty + B(U_s - U_\infty)} \quad (15)$$

Equation 15 gives the thrust loss in terms of the aerodynamic coefficients of the vanes and the deflection angle of the bypass stream. The factor $\overline{C_L^2}$ is generally not known a priori and needs to be computed after the lift coefficients of each vane pair have been found. When all the vane pairs produce the same C_L, we can connect this factor to the deflection angle via Eq. 8:

$$\overline{C_L^2} = C_L^2 = \left(\frac{\epsilon}{2 \beta \overline{\sin \phi}} \right)^2 \quad (16)$$

Equation 15 is valid for perfectly-expanded flow. Extension to imperfectly expanded flow is straightforward but beyond the scope of this paper. Clearly, the efficiency of this noise suppression scheme depends on the parasite drag coefficient C_{D_p} of the vane airfoils and the vane impact coefficient β. Both should be minimized. Minimization of β is constrained by the maximum lift coefficient before stall (Eq. 8). To avoid flow separation on the vanes, it would be prudent to use $C_{L_{\max}} \sim 1$. However, if the vanes were placed in a favorable pressure gradient (i.e., inside the convergent section of the bypass duct), larger values of $C_{L_{\max}}$ may be possible without flow separation. To minimize C_{D_p}, it is important to use thin, supercritical airfoils with good lift-to-drag ratios up to transonic Mach numbers. The problem of vanes placed inside the bypass duct lends itself to the shape optimization techniques recently developed for transonic airfoils [21]. The additional element of an externally-imposed favorable pressure gradient, which can delay shock losses and separation, creates the potential for efficiencies higher than those possible in a zero-pressure-gradient freestream.

The next step is to work out the relation between vane angle of attack α_j and lift coefficient C_{L_j}. Recalling that the effective downwash angle experienced by each vane pair is $(\epsilon \sin \phi_j)/2$,

$$C_{L_j} = a_{2D}(\alpha_j - \epsilon \sin \phi_j/2)$$

Inserting Eq. 8 and rearranging,

$$C_{L_j} + a_{2D} \beta \sin \phi_j \overline{C_L \sin \phi} = a_{2D} \alpha_j$$

This can be written as a system of simultaneous equations

$$A_{ij} C_{L_j} = a_{2D} \alpha_i \quad (17)$$

where

$$A_{ij} = \begin{cases} 2 \beta \sin \phi_j \sin \phi_i / N_v & , i \neq j \\ 1 + \beta \sin \phi_j / N_v & , i = j \end{cases} \quad (18)$$

4

Figure 3 plots the predictions of Eq. 18 for the take-off conditions listed in Table 3 and $U_\infty = 100$ m/s. It is assumed that C_L is same for all vanes so that the substitution of Eq. 16 can occur. The following coefficients are used: $\beta = 0.046$ (a value corresponding to case B60P-4Vg described later); $K = 0.4$; and $C_{D_p} = 0.01$ and 0.02. The lower value of C_{D_p} represents an efficient, supercritical airfoil at high-subsonic Mach number [21]. The higher value represents a standard thin airfoil at near-sonic Mach number [22]. With $C_{D_p} = 0.02$, the thrust loss is 0.5% at $\epsilon = 4°$, a deflection angle that is expected to be typical. Prediction of losses at cruise requires generalization of the above relations to imperfectly-expanded flows and use of engine cycle analysis to determine the exit velocities and Mach numbers. Details will be presented in future publications, but preliminary estimates indicate that the losses are similar to those predicted for takeoff.

Jet Noise Measurement

Noise testing was conducted in U.C. Irvine's Jet Aeroacoustics Facility [13], depicted in Fig. 4. Dual-stream jets, with flow conditions shown in Tables 1-3, were produced. The jets were composed of helium-air mixtures, which duplicate very accurately the fluid mechanics and acoustics of hot jets [24]. Jet nozzles were fabricated from epoxy resin using rapid-prototyping techniques. The pipe that fed the primary nozzle was able to flex, thus enabling coaxial or eccentric secondary flow passages.

Noise measurements were conducted inside an anechoic chamber using a one-eighth inch condenser microphone (Brüel & Kjær 4138) with frequency response of 140 kHz. The microphone was mounted on a pivot arm and traced a circular arc centered at the jet exit with radius of 100 effective (area-based) primary-jet diameters. Earlier experiments have determined that this distance is well inside the acoustic far field [25]. The polar angle θ ranged from 20° to 120° in intervals of 5° for $20° \leq \theta \leq 50°$ and 10° for the rest. Rotation of the nozzle assembly allowed variation of the azimuth emission angle. For most of the cases covered in this paper, the azimuth angle took the values $\phi = 0°$, 30°, 60°, and 90°. In a few cases, only the direction $\phi = 0°$ was surveyed.

The sound spectra were corrected for the microphone frequency response, free field response, and atmospheric absorption [26]. In our facility, rep-

etition of an experiment under varying temperature and relative-humidity conditions (typically from 20% to 50%) yields spectra that differ by at most 0.5 dB. Comparison of our single-jet spectra with those from NASA large-scale jet facilities, and with Tam's similarity spectra [27], shows excellent agreement both in the spectral shape and in the value of OASPL [28].

To be able to predict full-scale noise perceived by a human observer, the sound spectra were extrapolated to frequencies higher than those resolved in the experiment (140 kHz) using a decay slope of -30 dB/decade. This was done to resolve the audible spectrum for a full-scale engine. The PNL results are very insensitive on the assumed slope. Then the spectra were scaled up to engine size by dividing the laboratory frequencies by the scale factor $\sqrt{\mathcal{T}_{eng}/\mathcal{T}_{exp}}$. The full-scale engine diameter is the experimental diameter multiplied by this factor.

Earlier publications have described the conversion of spectra to effective perceived noise level (EPNL) measured by the takeoff monitor (i.e., a location on the extended centerline of the runway). Since this study includes the prediction of the sideline EPNL, for completeness we summarize the essential steps for predicting EPNL. The aircraft considered is twin-engine, each engine producing 90 kN of thrust. Two EPNL metrics are estimated: flyover and sideline (Fig. 5). The flyover flight path is straight and level at an altitude of 460 m. For the sideline noise, the flight path comprises a takeoff roll $x_{\text{LO}} = 1500$ m followed by a straight climb at angle $\gamma = 12°$ and $\alpha = 8°$. The sideline noise is monitored on a line parallel to the runway centerline and offset by 450 m. For both flyover and sideline predictions the aircraft velocity is 100 m/s ($M_\infty = 0.28$).

We now develop geometric relations for the observation distance and angles of the jet exhaust from an arbitrary point on the ground. Figure 6 shows the geometric constructions. Using the cartesian coordinate system (x, y, z), the airplane actual position is $(x', y', 0)$, the airplane retarded position is $(x, y, 0)$, and the observation point is at $(x_0, 0, z_0)$. The actual distance of the observer from the airplane is

$$ r' = \sqrt{(x' - x_0)^2 + y'^2 + z_0^2} $$

It can be shown easily that the retarded position is at a distance $M_\infty r'$ along the flight path behind the actual position. The observation distance at the

American Institute of Aeronautics and Astronautics

retarded position is

$$r \;=\; \sqrt{(x - x_0)^2 + y^2 + z_0^2} \qquad (19)$$

Assuming that the axis of the jet exhaust is aligned with the centerline of the airplane, the angle of the jet with respect to the horizontal is $\gamma + \alpha$. The axis of the exhaust intercepts the ground at location $(x_1, 0, 0)$, where

$$x_1 \;=\; x - \frac{y}{\tan(\gamma + \alpha)} \qquad (20)$$

From the geometry of the top diagram of Fig. 6, the polar observation angle is

$$\tan(\theta/2) \;=\; \sqrt{\frac{(p - b)(p - r)}{p(p - a)}} \qquad (21)$$

where

$$a = \sqrt{(x - x_1)^2 + z_0^2}$$

$$b = \frac{y}{\sin(\gamma + \alpha)}$$

$$p = \frac{1}{2}(a + b + r)$$

Referring to lower diagram of Fig. 6, the azimuth observation angle is

$$\tan(\phi) \;=\; \frac{z_0}{y} \cos(\gamma + \alpha) \qquad (22)$$

The flight path is computed at 0.5-sec intervals. For each observation time t, the distance $r(t)$, polar emission angle $\theta(t)$, and azimuth emission angle $\phi(t)$ are computed using the above procedures. The steps in assessing EPNL are the following:

1. For each t, the lossless, scaled-up spectrum corresponding to $\theta(t)$ and $\phi(t)$ is obtained. This step requires interpolation between spectra and, for polar angles outside the range covered in the experiment, moderate extrapolation. To enhance the accuracy of interpolation or extrapolation the spectra were smoothed using a Savitzky-Golay filter [29].

2. The spectrum is Doppler-shifted to account for the motion of the aircraft. The relations of McGowan & Larson [30] are used:

$$\frac{f_{\text{flight}}}{f_{\text{static}}} \;=\; \frac{1 + (M_c - M_\infty) \cos\theta}{1 + M_c \cos\theta}$$

The convective Mach number M_c is obtained from the empirical relations of Murakami & Papamoschou [23].

3. The spectrum is corrected for distance and atmospheric absorption. The distance correction is

$$-20 \log_{10} \left[\frac{(r/D_p)_{\text{eng}}}{(r/D_p)_{\text{exp}}} \right]$$

The absorption correction is applied for ambient temperature 29°C and relative humidity 70% (conditions of least absorption) using the relations of Bass et al. [26].

4. The spectrum is discretized into 1/3-octave bands and the perceived noise level (PNL) is computed according to Part 36 of the Federal Aviation Regulations [31].

5. The PNL is corrected for lateral attenuation according to SAE AIR 1571 [32]. This applies only to the sideline estimate.

6. The previous step gives the time history of perceived noise level, PNL(t). From it, the maximum level of PNL, PNLM, is determined. The duration of PNL exceeding PNLM-10 dB is calculated and the corresponding "duration correction" is computed according to FAR 36. The effective perceived noise level, EPNL, equals PNLM plus the duration correction. Our estimate of EPNL does not include the "tone correction", a penalty for excessively protrusive tones in the 1/3-octave spectrum which are absent from our spectra anyway.

For the sideline estimate, the EPNL is calculated at several observer positions $(x_0, 0, 400 \text{ m})$, with x_0 being incremented by 150 m from the lift off point. The maximum value of EPNL is then used as the estimate of sideline EPNL_{sl}. It is important to note that our experiments do not capture the effect of forward flight on jet acoustics. The only correction for forward flight is the Doppler shift of Step 2 above.

Acoustic Results

Our investigation encompassed three flows created by the combination of the nozzles shown in Fig. 7. For all the arrangements, the inner nozzle and plug were identical and resulted in an equivalent (area-based) exit diameter $D_{p,\text{eq}} = 10$ mm. The conditions of each flow are summarized in Tables 1-3. The notation Bxx is used for distinguishing each flow, with xx=10 × bypass ratio. The symbol P indicates a protrusion of the inner nozzle. For jet

American Institute of Aeronautics and Astronautics

B45, the bypass nozzle terminated in a gradual convergence uncharacteristic of actual bypass ducts. In cases B60 and B60P, the secondary nozzle was conical and formed a faster convergence. Case B60P, with a protruding inner nozzle, is the most realistic from a propulsion standpoint. We covered a variety of vane geometries as well as a few eccentric configurations. The vanes were fabricated from thin (0.13-mm) brass sheet and were attached to the outer surface of the inner nozzle with adhesive. Electrical tape (0.18-mm thickness) was wrapped around the vanes to produce a round leading edge. Early experiments showed that this procedure increases noise suppression, which suggests that the aerodynamics of the vanes improve by the rounding of the leading edge.

The parameter space relating to vane geometry is huge. Variables include the number of vanes, angle of attack, axial placement, azimuthal placement, vane airfoil, etc. A systematic variance of all these parameters would be extremely time-consuming and expensive. Instead, this study adopted a semi-random search approach with the goal of arriving quickly at configurations that provided good noise reduction. Then we tried small variations around those configurations to see if they were optimal. Table 4 summarizes our attempts. It describes the vane geometry, vane aerodynamic variables, and noise reduction. In our notation the suffix 2V indicates two vanes (single pair), 4V indicates four vanes (two pairs), and 6V indicates six vanes (three pairs). It is followed by a designation letter. ΔOASPL refers to the reduction in the peak level of OASPL. ΔEPNL$_{fo}$ and ΔEPNL$_{sl}$ refer to the reductions in effective perceived noise level for flyover and sideline, respectively. ΔEPNL$_{tot}$ is the sum of the last two numbers and can be used as a figure of merit. The baseline cases (-BASE) are coaxial clean nozzles. Next we provide a description of the main trends observed in the experiments.

Eccentricity

Figure 8 shows the polar directivity of the OASPL of B45-BASE and B45-ECC. The eccentric nozzle produced a substantial reduction in the peak value of OASPL. However, this was accompanied by an increase of sound at the high angles, which diminished the perceived-noise benefit. As a result, the flyover EPNL dropped by only 0.5 dB even though the peak OASPL reduced by 4.5 dB. The same trend was seen in the comparison of B60-BASE and B60-ECC. The source of the sound increase at the high

angles is not yet known, but it may be connected to the very thin flow passage on the top of the nozzle. These results suggest that an eccentric nozzle is not very attractive for high-bypass engines, notwithstanding the installation challenges.

Number of vanes

The number of vanes should not, by itself, be a significant parameter as long as we obtain the necessary vane impact coefficient β to deflect the flow. However, if we desire to shape the flow not only in the downward direction but also in the sideline direction, it seems advantageous to employ more than one pair of vanes. It is evident from Table 4 that the cases with a single pair of vanes (B45-2Va, B45-2Vb, B45-2Vc, and B60P-2Va) did not produce good sideline reduction (we cannot preclude the possibility that a single pair of vanes with complicated spanwise shape would produce better sideline suppression). The study therefore focused on combinations of two pairs of vanes. In a few instances, three vane pairs were investigated (B45-6Va, b, c, d). The results are not notably different from those with four vanes.

Angle of attack

Increasing the angle of attack of the vanes leads to higher vane lift and therefore stronger downward deflection of the bypass stream. This is expected to benefit noise reduction. Indeed, looking at the single-pair cases B45-2Va and B45-2Vb we note a reduction in the peak level of OASPL as α increases from 15° to 20°. The related OASPL plots are shown in Fig. 9. At the same time, however, we note an increase in OASPL for the large polar angles which hurts the perceived noise benefit.

This phenomenon is aggravated when multiple vane pairs are rotated uniformly at high angles of attack. The increase in noise at the large angles was a vexing issue until a curious solution was found: placing the vane pairs at dissimilar angles of attack. Specifically, the upper pair should be at an angle of attack lower than the lower pair. For example, Fig. 10 plots the OASPL directivity of B60-4Vd (two pairs of vanes, both at $\alpha = 15°$) and B60-4Ve (top pair at $\alpha = 10°$, bottom pair at $\alpha = 15°$). B60-4Ve showed no noise increase at the high angles, and its EPNL benefit was much higher than that of B60-4Vd, even though the total lift of the vanes was less. The same holds for combinations with $\alpha=10°$ and 12°; see cases B60-4Vb and B60-4Vc. The ad-

American Institute of Aeronautics and Astronautics

vantageous effect of dissimilar angles of attack was discovered in the B60 experiments, which occurred after the B45 experiments were completed. It is expected that this approach would also have worked in the B45 nozzle.

The reason for the advantage of dissimilar angles of attach is not yet clear. It may have to do with a more even distribution of aerodynamics load on the vanes, which in turn leads to smoother turning of the flow, with less non-uniformity, near the nozzle exit. To appreciate this we must consider the influence of one pair on the other, something that is lacking in the analysis of pp. 3-5. Assuming that we have two pairs of vanes not too far apart in the azimuthal direction, the bottom pair is likely to experience some relief of the aerodynamic load because the upper pair is already turning the flow downward. The upper pair is unlikely to get much relief from the bottom pair because the upper pair is bounded on the top by straight walls. Thus, when we install two pairs at the same α, the upper pair will probably be more loaded than the bottom pair. Decreasing α of the upper pair distributes the load more evenly.

Azimuth angle

Our tests show that sound reduction is very sensitive on the azimuthal position of the vanes. With a single vane pair, moving the vanes from $\phi = 90°$ to $\phi = 75°$ (B45-2Vb and B45-2Vc) resulted in a substantial loss of the acoustic benefit. With two vane pairs, each vane along radial lines ($\delta\phi = 0°$), the optimal position was around $\phi_1 = 70°$ and $\phi_2 = 110°$. If those two angles were shifted uniformly upwards or downwards by more than 10° the acoustic benefit dropped substantially. Compare the OASPL plots of B45-4Vb and B45-4Va in Fig. 11. Vane anhedral did not help in any case so far, whereas vane dihedral helped in one case, B60-4Vj. This configuration, with $\phi_1 = 70°$, $\delta\phi_1 = 0°$ $\phi_2 = 120°$, and $\delta\phi_2 = 20°$, provided the best overall benefit of the B60 series but was only marginally better than case B60-4Ve with radial vanes.

Axial placement and nozzle shape

The vanes are expected to be most effective in deflecting the bypass stream when they are placed very close to the exit of the bypass duct. If they are installed too deep in the bypass duct their effect will be lessened or cancelled by pressures developing on the nozzle inner surfaces. At the same time, one should be mindful that the exit of the bypass duct is typically at near-sonic conditions, a flow regime conducive to substantial losses. Also, strong shock formation around the vanes could become an additional source of noise.

A glance at Table 4 shows that the acoustic benefit of the vanes gets stronger as we shift from B45 to B60 to B60P. This is not related to the increase in bypass ratio – that increase was incidental to the nozzle diameters used. Instead, it has to do with the shape and termination of the bypass duct. In case B45, the duct is slowly converging and the Mach number is high in the proximity of the duct exit. In cases B60 and B60P, the duct converges fast and the Mach number drops rapidly with distance upstream of the exit. To install the vanes in a subsonic environment in nozzle B45, their trailing edges were 3.2 mm (80% of the annulus height) upstream of the nozzle exit. This means that they lost some of their effectiveness. In cases B60 and B60P, the average Mach number over the vanes was subsonic even with the vane trailing edges coinciding with the duct exit.

In case B45, moving the vanes further upstream resulted in a significant loss of the acoustic benefit. Compare cases B45-4Vc and B45-4Vd. The vane impact coefficient was not significantly reduced (the loss in dynamic pressure was offset to some degree by the larger size of the vanes), which suggests that the vane effectiveness was reduced due to transfer of force on the nozzle walls. In case B60P, a small (1-mm) shift of the vane trailing edge upstream of the duct exit resulted in better noise reduction. Compare cases B60P-4Va and B60P-4Vg. The average vane Mach number was reduced from 0.76 to 0.65, but the vane remained in very close proximity to the duct exit. The noise reduction may thus be attributed to weakening of shocks around the vane.

In comparing the overall acoustic performance of the B60 and B60P cases, we observe a general benefit of having the inner nozzle protrude. The protrusion offers a little more distance for the bypass stream to shift downward as it approaches the end of the primary potential core. In other words, for the same deflection angle, the protrusion allows a thicker concentration of secondary flow at the end of the primary potential core. This could be the reason for the better performance of the vanes in B60P relative to B60. Realistic bypass ducts have fast convergence and terminate upstream of the end of the core nozzle, which bodes well for the application of this technique on separate-flow bypass engines.

American Institute of Aeronautics and Astronautics

Best case

It is worthwhile examining in more detail some acoustic features of the best case of this paper, B60P-4Vg. Figure 12 shows the sound spectra at $\phi = 0°$ and $\phi = 60°$ and at polar angles $\theta = 20°$ (the angle closest to the jet axis), $\theta = 30°$ (direction of peak emission) and $\theta = 90°$. The frequency has been scaled for a full-size thrust of 90 kN. The direction $\phi = 0°$ is pertains to flyover noise, and the direction $\phi = 60°$ influences strongly sideline noise. Very close to the jet axis, noise reduction in the downward direction exceeds 10 dB in the frequency band 100-500 Hz. In the direction of peak emission, noise reduction in that band is around 7 dB at $\phi = 0°$ and 4 dB at $\phi = 60°$. In the lateral direction, no changes are detected between the baseline case and the case with vanes.

Figure 13 plots the OASPL polar directivity at azimuth angles $\phi = 0°$ and $60°$. In the downward direction, the peak OASPL reduces by 4.7 dB. In the sideline direction, the corresponding reduction is 3.1 dB. To get a more complete picture of the dependence of sound reduction on azimuth angle, Fig. 14 shows the OASPL reduction versus ϕ for various polar angles. As expected, for small polar angles the acoustic benefit shows a gradual reduction with increasing ϕ. Of course, the OASPL is not a good descriptor of perceived noise. To assess the perceived noise variance with azimuth angle, we plot in Fig. 15 the "flyover" EPNL reduction versus ϕ. This is purely an academic exercise; the only EPNL pertinent to flyover noise is for $\phi = 0°$. To understand better the significance of Fig. 15, imagine an airplane flying straight and level but at different bank angles ϕ (a situation that would never happen in certification). Figure 15 shows that the perceived noise benefit gradually decline with increasing ϕ, starting at 3.3 dB at $\phi = 0°$ and ending with 1.1 dB at $\phi = 90°$. Interestingly, both the OASPL and the EPNL indicate that there is a benefit, albeit small, at $\phi = 90°$.

Finally Fig. 16 plots the time history of flyover perceived noise level. The advantage of B60P-4Vg over the baseline lies both in the reduced level of the maximum level of PNL (PNLM) and the shorter duration of the 10 db down level. For times past the occurrence of PNLM, noise suppression becomes very pronounced. The corresponding emission angles are close to the jet axis and the acoustic field is dominated by noise generated from large-scale structures. A short time prior to the occurrence of

PNLM, the emission angles are large so noise from fine-scale turbulence dominates. For those times, the PNL curves of B60P-4Vg and B60P-BASE coincide.

General Trend

One wonders if there are any unifying trends in all the data collected so far. Recall that the effectiveness of this noise suppression technique is expected to depend strongly on the deflection angle of the bypass stream ϵ. It is therefore natural to try correlate the acoustic benefit versus that angle. In this sense, the best metric of noise reduction is the reduction in peak OASPL at $\phi = 0°$. Perceived noise depends on many additional factors, such as noise emitted at large angles, that cannot be captured by a simple correlation. Figure 17 plots the reduction in peak level of OASPL versus the *estimated* deflection angle of each arrangement with vanes (Eq. 8). There is a definite trend of increasing noise suppression with increasing deflection angle. There is also appreciable scatter, which indicates either an error in the estimate of ϵ or the possibility that, with the same ϵ, we can have various levels of effectiveness in reducing noise. One case that does not fit the trend at all (B45-4Vb) employed vanes at high azimuth angles. It is possible that, under these conditions, the bypass stream breaks up into multiple jets and is thus unable to cover adequately the noise source region of the primary jet.

Aerodynamics of Best Case

We now discuss some elements of the aerodynamics of the best arrangement, case B60P-4Vg. Figure 18 shows the vane placement in relation to the coordinates of the bypass duct. Based on one-dimensional approximation of the internal flow, the Mach numbers at the leading and trailing edges of each vane were calculated to be 0.55 and 0.75, respectively. Thus, each vane experienced an average "freestream" Mach number of 0.65.

Based on the vane geometry shown in Table 1, the vane impact factor was $\beta = 0.046$. Assuming $a_{2D} = 0.08$ deg^{-1}, the lift coefficient of the top vane pair was $C_{L_1} = 0.7$ and the lift coefficient of the bottom vane pair was $C_{L_2} = 1.0$. The deflection angle is estimated to be $\epsilon = 4.5°$. Using Eq. 15 with $C_{D_p} = 0.02$ (a conservative value), $K = 0.4$, $U_\infty = 100$ m/s, and the conditions of Table 3, the thrust loss with vanes deflected is estimated at 0.5%. With the

American Institute of Aeronautics and Astronautics

vanes deactivated ($\alpha = 0°$), the thrust loss is 0.15%.

Based on the calculated pressure distribution in the clean duct, each vane was subjected to a normalized pressure gradient

$$\frac{c}{p}\frac{dp}{dx} = -0.3$$

with the reference pressure p evaluated at the leading edge of the vane. This is a very strong favorable gradient that is likely to improve airfoil performance, especially at high angles of attack.

Concluding Remarks

Our parametric study of bypass deflectors has produced data that provide guidance for optimal arrangements and shed some light on the physics of the deflectors. The principal observations are as follows:

1. A bypass nozzle with rapidly convergent area creates the best operational environment for the vanes. It allows the vanes to be installed very close to the exit of the bypass duct while remaining in a subsonic environment.

2. Using more than one pair of vanes allows more flexibility in the simultaneous reduction of downward and sideline noise.

3. When using two pairs of vanes, it is advantageous to place the top pair at a smaller angle of attack than the bottom pair. This has been shown to prevent a rise in the noise emitted at the large polar angles.

4. For a single pair of vanes, the best azimuthal placement is around $\phi = 90°$

5. For two pairs of vanes, the best azimuthal placement is around $\phi_1 = 70°$ and $\phi_2 = 110°$

There is a strong correlation between the estimated deflection angle of the bypass stream and the noise reduction in terms of OASPL. Nevertheless, many details escape explanation. That's because this study was essentially blind, without knowledge of the mean flow field. The ideal experiment would combine the sound survey with a thorough mapping of the mean velocity field. However, this is too impractical and expensive. We plan to survey a few of the best and worst configurations to gain understanding on the connection between the mean flow and the acoustics. It is hoped that computations will come to the stage where they can predict in "real time" the mean flow field issuing from nozzles with deflectors. This would be an invaluable tool in our quest for optimization and search for the physical reasons for many of the phenomena observed here.

Acknowledgments

References

[1] Tam, C.K.W., and Chen, P., "Turbulent Mixing Noise from Supersonic Jets," *AIAA Journal*, Vol. 32, No. 9, 1994, pp. 1774-1780.

[2] Tam, C.K.W., "Jet Noise: Since 1952," *Theoretical and Computational Fluid Dynamics,*" Vol. 10, 1998, pp. 393-405.

[3] Saiyed, N.H., Mikkelsen, K.L., and Bridges, J.E., "Acoustics and Thrust of Separate-Flow High-Bypass-Ratio Engines," *AIAA Journal*, Vol. 41, No. 3, 2003, pp. 372-378.

[4] McLaughlin, D.K., Morrison, G.D., and Troutt, T.R., "Experiments on the Instability Waves in a Supersonic Jet and their Acoustic Radiation," *Journal of Fluid Mechanics*, Vol. 69, No. 11, 1975, pp. 73-95.

[5] Troutt, T.R., and McLaughlin, D.K., "Experiments on the Flow and Acoustic properties of a Moderate Reynolds Number Supersonic Jet, " *Journal of Fluid Mechanics*, Vol. 116, March 1982, pp. 123-156.

[6] Tam, C.K.W., and Burton, D.E., "Sound Generated by Instability Waves of Supersonic Flows. Part 2. Axisymmetric Jets," *Journal of Fluid Mechanics*, Vol. 138, 1984, pp. 249-271

[7] Seiner, J.M., Bhat, T.R.S, and Ponton, M.K., "Mach Wave Emission from a High-Temperature Supersonic Jet," *AIAA Journal*, Vol. 32, No. 12, 1994, pp. 2345-2350.

[8] Mitchell, B.E., Lele, S.K., and Moin, P. (1997), "Direct Computation of Mach Wave Radiation in an Axisymmetric Supersonic Jet," *AIAA Journal*, Vol. 35, No. 10, pp. 1574-1580.

[9] Mankbadi, R.R., Hixon, R., Shih, S.-H., and Povinelli, L.A., "Use of Linearized Euler Equations for Supersonic Jet Noise Prediction," *AIAA Journal*, Vol.36, No.2, 1998, pp. 140-147.

[10] Crighton, D.G. and Huerre, P., "Shear-Layer Pressure Fluctuations and Superdirective Acoustic Sources," *Journal of Fluid Mechanics*, Vol. 220, 1990, pp. 355-368.

[11] Avital, E.J., Sandham, N.D, and Luo, K.H., "Mach Wave Radiation in Mixing Layers. Part I: Analysis of the Sound Field," *Theoretical and Computational Fluid Dynamics*, Vol. 12, 1998, pp. 73-90.

[12] Freund, J.B., "Noise Souces in a Low-Reynolds-Number Turbulent Jet at Mach 0.9," *Journal of Fluid Mechanics*, Vol. 438, 2001, pp. 277-305.

[13] Papamoschou, D. and Debiasi, M., "Directional Suppression of Noise from a High-Speed Jet," *AIAA Journal*, Vol. 39, No. 3, 2001, pp. 380-387.

[14] Papamoschou, D. and Debiasi, M., "Conceptual Development of Quiet Turbofan Engines for Supersonic Aircraft," *AIAA Journal of Propulsion and Power,*, Vol. 18, No.2, 2003, pp. 161-169.

[15] Papamoschou, D., "A New Method for Jet Noise Reduction in Turbofan Engines," AIAA-2003-1059.

[16] Papamoschou, D., "Engine Cycle and Exhaust Configurations for Quiet Supersonic Propulsion," AIAA-2002-3917, to appear in the *AIAA Journal of Propulsion and Power*.

[17] Panda J. and Seasholtz, R.G., "Experimental Investigation of Density Fluctuations in High-Speed Jets and Correlation with Generated Noise," *Journal of Fluid Mechanics,* Vol.450, Jan. 2002, pp.97-130.

[18] Hileman, J. and Samimy, M. "Turbulence Structures and the Acoustic Far Field of a Mach 1.3 Jet," *AIAA Journal*, Vol.39, No.9, 2001, pp.1716-27.

[19] Narayanan, S., Barber, T.J., and Polak, D.R., "High Subsonic Jet Experiments: Turbulence and Noise Generation Studies," *AIAA Journal*, Vol. 40, No. 3, 2002, pp. 430-437.

[20] Shevell, R.S., "Fundamentals of Flight," Prentice Hall, 1989, pp. 146-147, 186.

[21] Kim, S., Alonso, J.J., and Jameson, A., "Design Optimization of High-Lift Configurations Using a Viscous Continuous Adjoint Method," AIAA-2002-0844, January 2002.

[22] Ladson, C.L., "Two-Dimensional Airfoil Characteristics of Four NACA 6A-Series Airfoils at Transonic Mach Numbers up to 1.25," NACA RM L57F05, August 1957.

[23] Murakami, E. and Papamoschou, D., "Eddy Convection in Supersonic Coaxial Jets," *AIAA Journal*, Vol. 38, No.4, 2000, pp. 628-635.

[24] Kinzie, K.W., and McLaughlin, D.K., "Measurements of Supersonic Helium/Air Mixture Jets," *AIAA Journal,* Vol. 37, No. 11, 1999, pp. 1363-1369.

[25] Papamoschou, D., and Debiasi, M. "Noise Measurements in Supersonic Jets Treated with the Mach Wave Elimination Method," *AIAA Journal*, Vol. 37, No. 2, 1999, pp. 154-160.

[26] Bass, H.E., Sutherland, L.C., Zuckerwar, A.J., Blackstock, D.T., and Hester, D.M., "Atmospheric Absorption of Sound: Further Developments, " *Journal of the Acoustical Society of America,* Vol. 97, 1995, pp. 680-683.

[27] Tam, C. K. W., Golebiowski, M., and Seiner, J., "On the Two Components of Turbulent Mixing Noise from Supersonic Jets," AIAA-96-1716, 1996.

[28] Proceedings of the Jet Noise Workshop, NASA Glenn Research Center, November 7-9, 2000. NASA CP-2001-211152.

[29] Savitzky, A. and Golay, M.J.E. "Smoothing and Differentiation of Data by Simplified Least Squares Procesures," *Analytical Chemistry*, Vol. 36, No. 8, 1964, pp. 1627-.

American Institute of Aeronautics and Astronautics

[30] McGowan, R.S. and Larson, R.S., "Relationship Between Static, Flight and Simulated Flight Jet Noise Measurements," *AIAA Journal*, Vol. 22, No. 4, 1984, pp. 460-464.

[31] "Noise Standards: Aircraft Type and Airworthiness Certificiation," Federal Aviation Regulations Pt. 36, Federal Aviation Administration, Jan. 2001.

[32] Society of Automotive Engineers Aerospace A21 committee. Prediction of Lateral Attenuation of airplane noise during takeoff and landing. Information Report - SAE AIR-1751. March 1981.

Table 1   Exit conditions for B45

Quantity	Primary	Secondary
Nozzle diameter (mm)	14.2	23.6
Plug diameter (mm)	10.0	-
Lip thickness (mm)	0.8	-
Protrusion (mm)	0.0	-
Velocity (m/s)	500	350
Mach number	0.90	0.95
Bypass ratio	-	4.5

Table 2   Exit conditions for B60

Quantity	Primary	Secondary
Nozzle diameter (mm)	14.2	25.4
Plug diameter (mm)	10.0	-
Lip thickness (mm)	0.8	-
Protrusion (mm)	0.0	-
Velocity (m/s)	460	335
Mach number	0.86	0.95
Bypass ratio	-	6.0

Table 3   Exit conditions for B60P

Quantity	Primary	Secondary
Nozzle diameter (mm)	14.2	25.4
Plug diameter (mm)	10.0	-
Lip thickness (mm)	0.8	-
Protrusion (mm)	13.0	-
Velocity (m/s)	460	335
Mach number	0.86	0.95
Bypass ratio	-	6.0

Table 4   Summary of results

Case	c	w	x_{te}	α_1	α_2	α_3	ϕ_1	ϕ_2	ϕ_3	$\delta\phi_1$	$\delta\phi_2$	$\delta\phi_3$	β	M_v	ΔOASPL	ΔEPNL$_{fo}$	ΔEPNL$_{sl}$	ΔEPNL$_{tot}$
B45-BASE															0.0	0.0	0.0	0.0
B45-ECC															4.5	0.5	-	-
B45-2Va	3.9	3.9	-3.2	15	-	-	90	-	-	0	-	-	0.022	0.71	2.7	1.2	0.7	1.8
B45-2Vb	3.9	3.9	-3.2	20	-	-	90	-	-	0	-	-	0.022	0.71	3.5	1.6	-0.2	1.5
B45-2Vc	3.9	3.9	-3.2	20	-	-	75	-	-	0	-	-	0.022	0.71	3.3	1.2	-0.8	0.5
B45-4Va	3.9	3.9	-3.2	10	10	-	70	110	-	0	0	-	0.044	0.71	4.1	1.5	-	-
B45-4Vb	3.9	3.9	-3.2	10	10	-	90	130	-	0	0	-	0.044	0.71	0.8	0.2	0.3	0.5
B45-4Vc	3.9	3.9	-3.2	15	15	-	70	110	-	0	0	-	0.044	0.71	4.6	1.7	0.7	2.4
B45-4Vd	4.1	4.1	-6.4	15	15	-	70	110	-	0	0	-	0.039	0.61	3.1	1.0	-	-
B45-6Va	3.9	3.9	-3.2	10	10	10	60	90	120	0	0	0	0.066	0.71	4.2	2.0	0.6	2.5
B45-6Vb	3.9	3.9	-3.2	10	10	10	70	90	110	0	0	0	0.066	0.71	3.8	1.6	1.1	2.6
B45-6Vc	3.9	3.9	-3.2	10	10	10	70	90	110	0	0	0	0.066	0.71	4.1	1.2	-	-
B45-6Vd	3.9	3.9	-3.2	10	10	10	60	80	100	0	0	0	0.066	0.71	3.9	1.4	0.6	2.1
B60-BASE	0.0	0.0	0.0												0.0	0.0	0.0	0.0
B60-ECC	0.0	0.0	0.0												2.9	0.4	-	-
B60-4Va	4.6	4.6	0.0	10	10	-	70	110	-	0	0	-	0.052	0.76	4.3	1.6	1.2	2.8
B60-4Vb	4.6	4.6	0.0	12	12	-	70	110	-	0	0	-	0.052	0.76	4.3	1.7	-	
B60-4Vc	4.6	4.6	0.0	12	10	-	70	110	-	0	0	-	0.052	0.76	4.4	2.1	1.2	3.3
B60-4Vd	4.6	4.6	0.0	15	15	-	70	110	-	0	0	-	0.052	0.76	5.1	1.2	-	-
B60-4Ve	4.6	4.6	0.0	15	10	-	70	110	-	0	0	-	0.052	0.76	4.5	2.6	1.0	3.6
B60-4Vf	4.6	4.6	0.0	15	12	-	70	110	-	0	0	-	0.052	0.76	5.2	2.2	1.2	3.4
B60-4Vg	4.6	4.6	0.0	15	10	-	70	110	-	0	20	-	0.052	0.76	5.4	2.6	0.4	3.0
B60-4Vh	4.6	4.6	0.0	15	10	-	70	120	-	0	0	-	0.052	0.76	4.9	1.8	1.5	3.3
B60-4Vi	4.6	4.6	0.0	15	10	-	70	120	-	0	-30	-	0.052	0.76	4.7	1.5	1.5	3.0
B60-4Vj	4.6	4.6	0.0	15	10	-	70	120	-	0	20	-	0.052	0.76	4.9	2.5	1.3	3.8
B60-4Vk	4.6	4.6	0.0	15	10	-	70	120	-	20	20	-	0.052	0.76	5.1	2.4	0.5	3.0
B60P-BASE	0.0	0.0	0.0												0.0	0.0	0.0	0.0
B60P-2Va	4.6	4.6	0.0	15	-	-	90	-	-	0	-	-	0.026	0.76	3.8	2.2	0.5	2.8
B60P-4Va	4.6	4.6	0.0	15	10	-	70	110	-	0	0	-	0.051	0.76	3.9	2.9	1.8	4.7
B60P-4Vb	4.6	4.6	0.0	15	10	-	70	110	-	-10	0	-	0.051	0.76	4.8	3.4	-	-
B60P-4Vc	4.6	4.6	0.0	10	15	-	70	110	-	0	0	-	0.051	0.76	4.2	2.3	-	-
B60P-4Vd	4.6	4.6	0.0	15	10	-	60	110	-	0	0	-	0.051	0.76	5.4	3.9	1.0	4.8
B60P-4Ve	4.6	4.6	0.0	15	10	-	70	120	-	0	20	-	0.051	0.76	3.9	2.7	1.9	4.6
B60P-4Ve	4.6	4.6	0.0	15	10	-	60	110	-	30	0	-	0.051	0.76	3.9	2.9	0.9	3.9
B60P-4Vf	4.6	4.6	0.0	15	10	-	70	120	-	0	10	-	0.051	0.76	3.9	2.7	-	-
B60P-4Vg	4.8	4.8	-1.6	15	10	-	70	110	-	0	0	-	0.046	0.65	4.7	3.3	2.0	5.3

Dimensions in mm; angles in deg; noise in dB

American Institute of Aeronautics and Astronautics
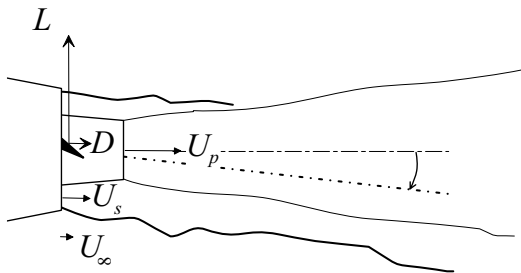
Fig.1 Deflection of the bypass stream.

Fig.2 Vane geometry.
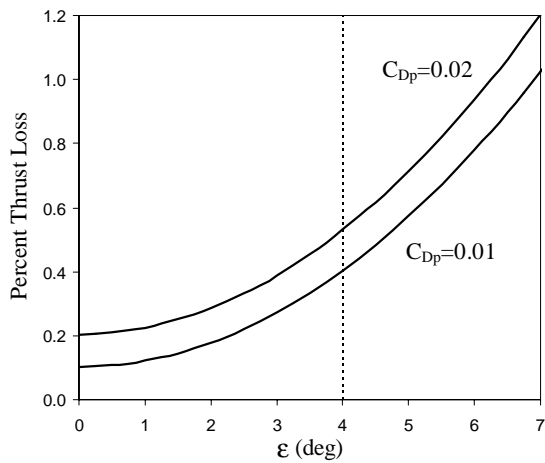
Fig.3 Prediction of thrust loss for flow similar to B60P-4Vg.

Fig.4 Jet aeroacoustic facility.
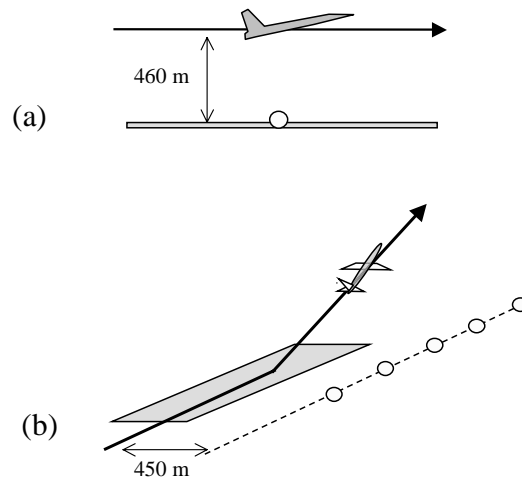
Fig.5 Measurement locations for perceived noise evaluation: (a) flyover; (b) sideline.

American Institute of Aeronautics and Astronautics
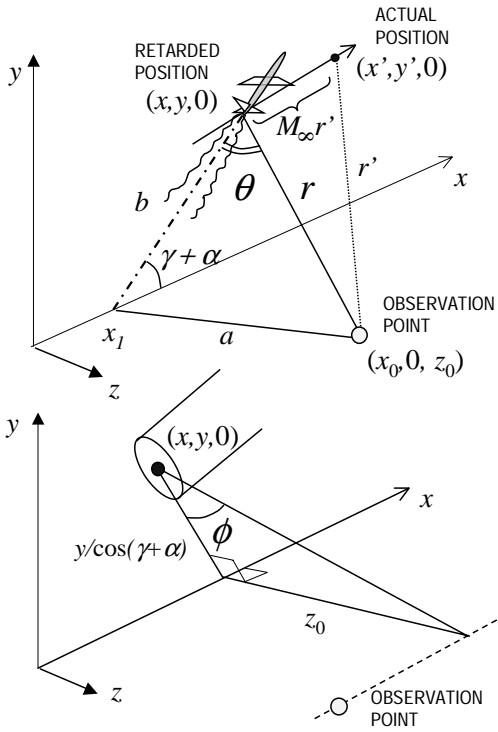
Fig.6 Geometric construction for observation distance and angles.
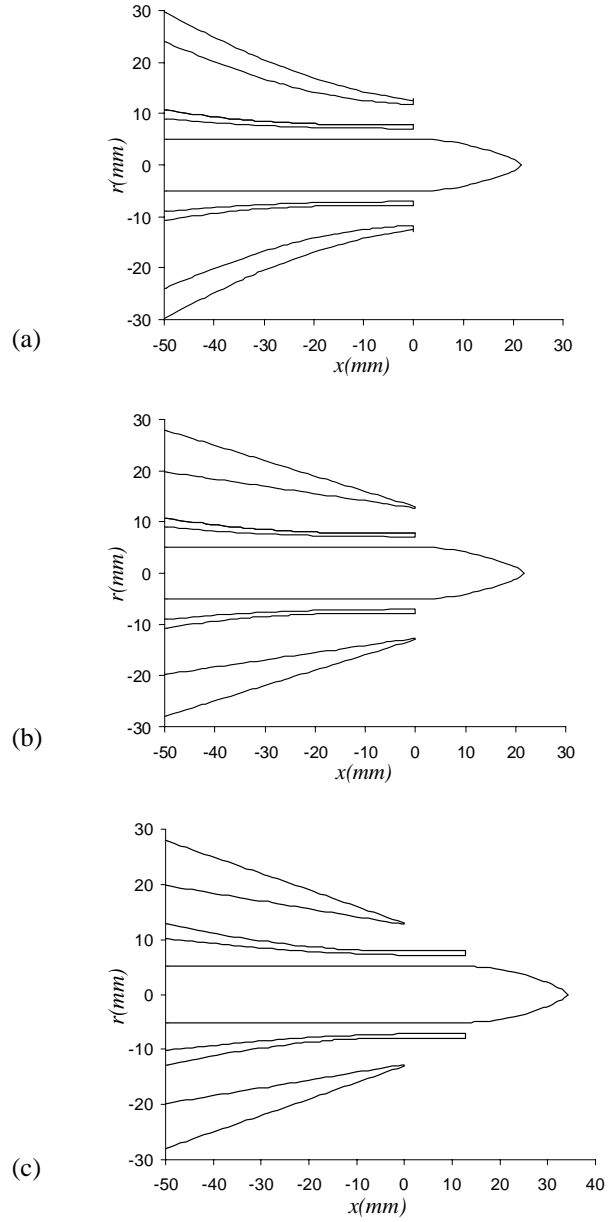
Fig.7 Nozzle geometry for: (a) B45; (b) B60; and (c) B60P.
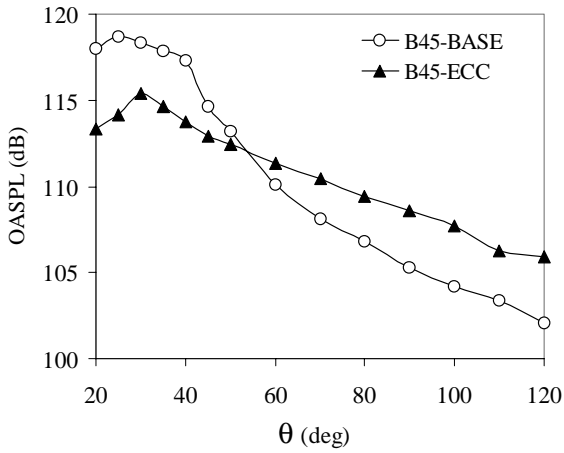
Fig.8 Directivity of OASPL at $\phi = 0°$ for baseline and eccentric cases.
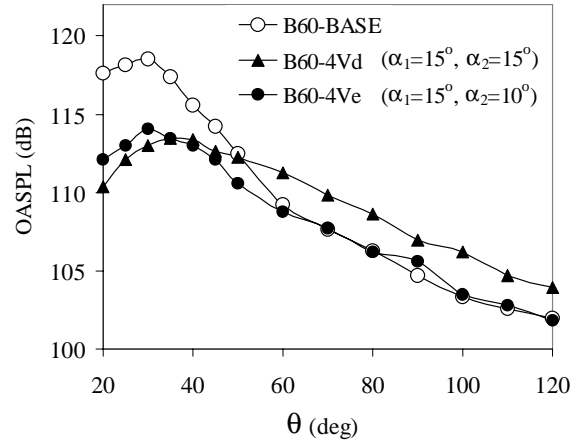
Fig.10 Effect of vane angle of attack on downward OASPL of jet with two pairs of vanes.
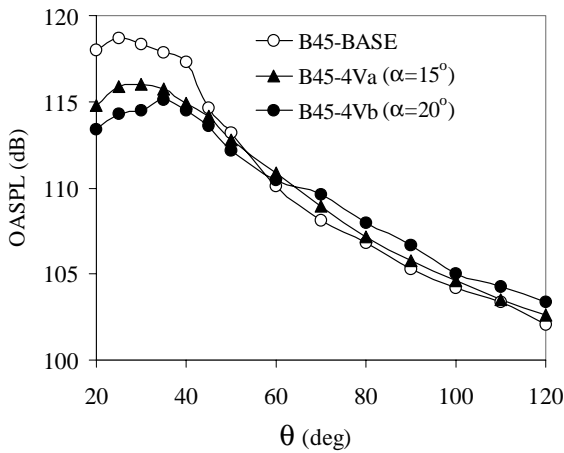
Fig.9 Effect of vane angle of attack on downward OASPL of jet with single pair of vanes.
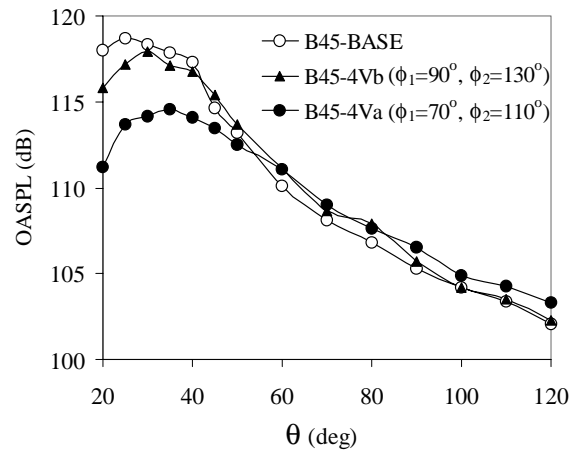
Fig.11 Effect of vane azimuth angle on downward OASPL of jet with two pairs of vanes.

16

(a)

(b)

(c)
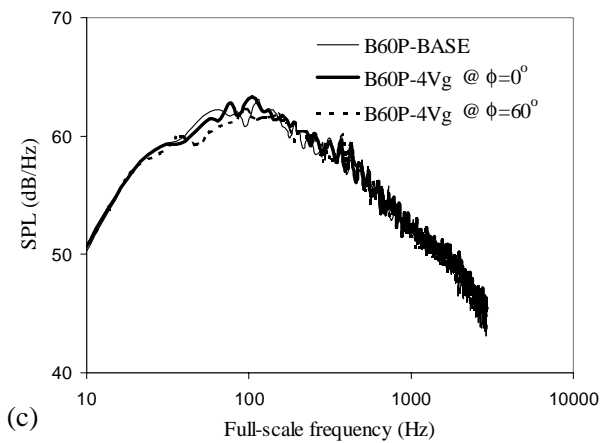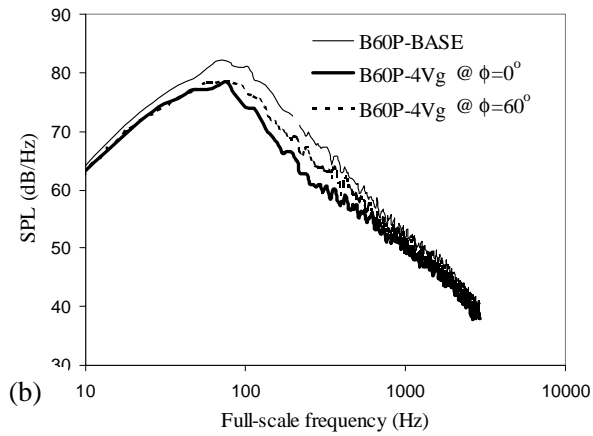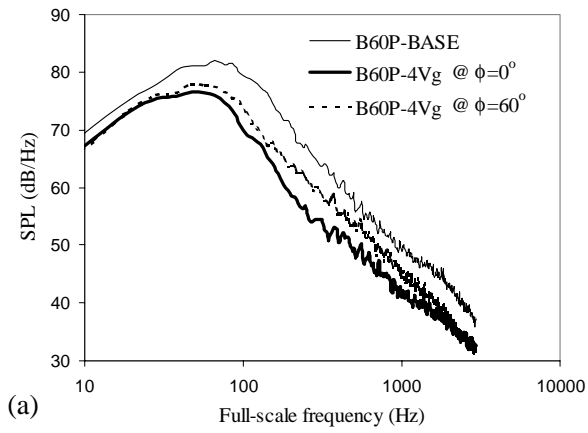
Fig.12 Far-field spectra of best case at (a) $\theta = 20°$; (b) $\theta = 30°$; and (c) $\theta = 90°$.
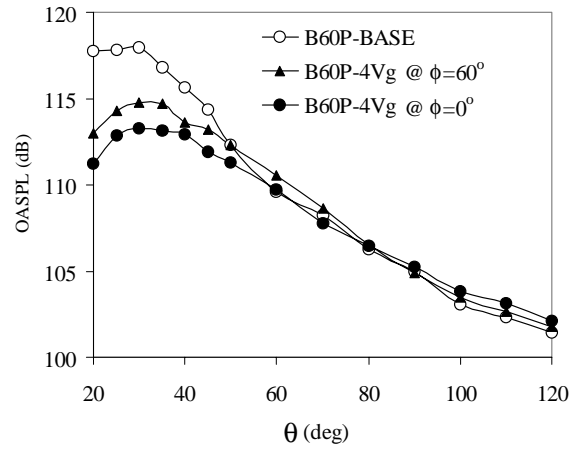
Fig.13 OASPL versus θ of case B60P-4Vg at azimuth angles $\phi = 0°$ and $60°$.
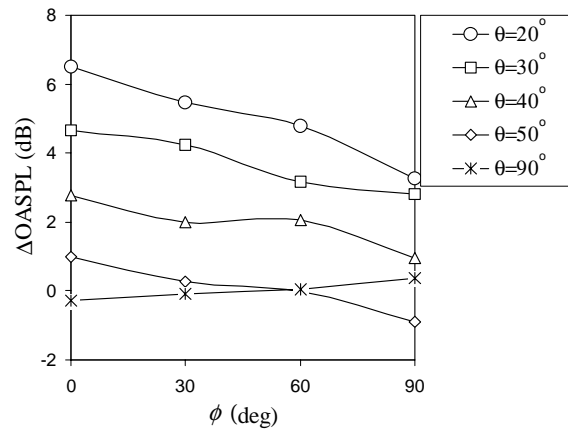
Fig.14 Reduction in OASPL versus ϕ for case B60P-4Vg at various polar angles.

American Institute of Aeronautics and Astronautics
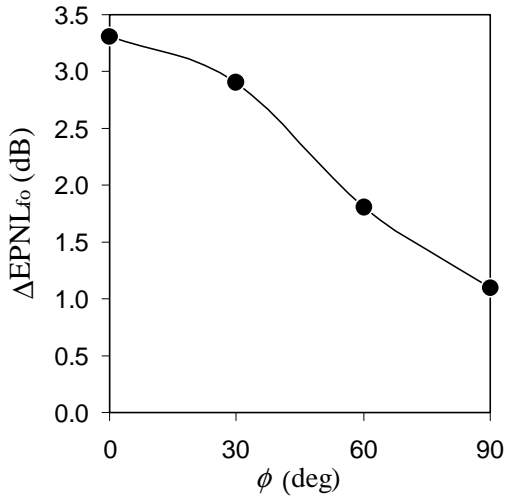
Fig.15 Reduction in flyover EPNL for case B60P-4Vg at various azimuth angles (aircraft bank angles).
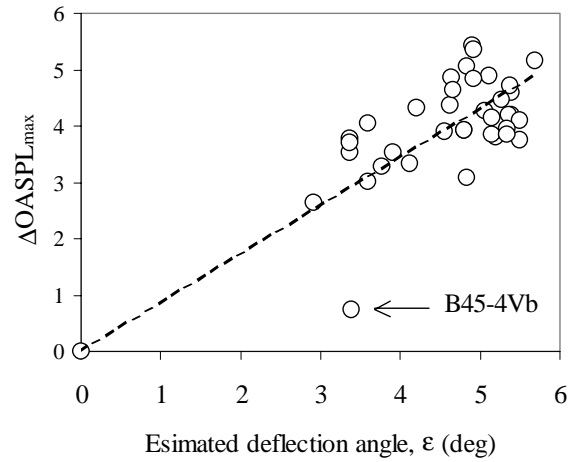
Fig.17 Reduction in peak value of OASPL versus estimated deflection angle of bypass stream.
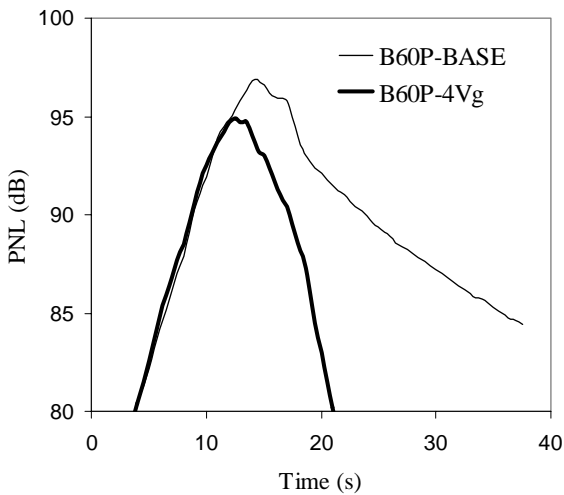
Fig.16 History of flyover PNL for B60P-BASE and B60P-4Vg.
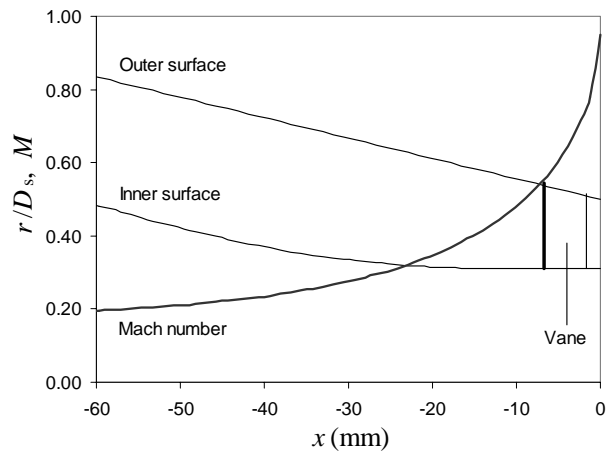
Fig.18 Internal flow of case B60P-4Vg.